NUMERICAL SIMULATIONS OF TURBULENT TRAPPING IN THE WEAK BEAM-PLASMA INSTABILITY,

by

K. Theilhaber, G. Laval and D. Pesme

Memorandum No. UCB/ERL-M86/50.

5 June 1986

ELECTRONICS RESEARCH LABORATORY
College of Engineering
University of California, Berkeley, CA 94720

NUMERICAL SIMULATIONS OF TURBULENT TRAPPING IN THE WEAK BEAM-PLASMA INSTABILITY

by

K. Theilhaber, G. Laval and D. Pesme

Memorandum No. UCB/ERL M86/50

5 June 1986

ELECTRONICS RESEARCH LABORATORY

College of Engineering
University of California, Berkeley
94720

NUMERICAL SIMULATIONS OF TURBULENT TRAPPING IN THE WEAK BEAM-PLASMA INSTABILITY.

K.Theilhaber.
Plasma Theory and Simulation Group,
Electronics Research Lab,
University of California,
Berkeley, CA 94720,USA

G. Laval and D. Pesme.
Centre de Physique Theorique,
Ecole Polytechnique,
91128 Palaiseau, France.

ABSTRACT.

Numerical simulations of the weak beam-plasma instability were done in the turbulent regime where small-scale trapping is a dominant feature of the instability, a regime with behavior not predicted by quasilinear theory. It occurs when the trapping frequency $\nu = (k^2 D)^{1/3}$ is larger than the growth rate γ_k of the instability. The results of the simulations were compared with those of a specific model of the turbulence, the so-called "turbulent trapping" model, which gives precise formulas for the particle correlation functions, and predicts a growth rate well enhanced over the quasilinear value. It was found that the model gives accurate predictions for the correlation functions, and thus provides a good description of the turbulent structure of phase space. On the other hand, while growth rates were enhanced over the quasilinear values, the enhancements observed are smaller than expected from the quantitative predictions of the model. Further work is necessary to determine whether this discrepancy is a failing of the turbulent trapping model, or the result of the numerical limitations of our computational scheme.

I. INTRODUCTION.

Since its creation over 20 years ago ([1]), quasilinear theory has been accepted as the valid description of weakly turbulent plasmas where wave-particle interactions dominate, with as central paradigm the weak, warm-beam-plasma instability. It is only relatively recently that the rigor of its derivation and its range of validity in the one-dimensional case have been questioned by J.C. Adam, G. Laval and D. Pesme (ALP([2],[3],[4],[5])). Their work demonstrates the existence of a new regime existing within the accepted limits of quasilinear theory, in which both the growth-rate and the velocity-space diffusion should be enhanced over their quasilinear values.

This conclusion is based on the existence of strong mode-coupling effects between resonant waves, due to the self-consistency of the electric field, effects which occur when the resonance broadening frequency, $\nu_k \equiv (k^2 D^{ql})^{1/3}$, is larger than the quasilinear growth-rate γ_k^{ql}. In this regime, a set of mode coupling-terms, arranged in an infinite series, becomes of the same order as the quasilinear term. This arises because of the partial trapping of the beam particles by the waves on a time scale $\nu_k^{-1} \ll (\gamma_k^{ql})^{-1}$, a process which generates a harmonic series of sidebands or "quasimodes", that is non-resonant perturbations of the beam distribution function, at the harmonic frequencies $\omega = n\omega_k$ and at the wave numbers nk. These quasimodes do not satisfy Poisson's equation, but perturb particles for which the resonance condition of the fundamental, $\omega_k = kv$, continues to be satisfied. Because of this invariance of the resonance condition, the mode-coupling coefficients are large, even though the coupling takes place via small, non-resonant sidebands. Thus, the cascade of the quasimodes beating back into the fundamental leads, over a few e-foldings, to effects of the same order as the usual wave-particle interaction. In particular, under this regime the statistical properties of the electric field strongly deviate from Gaussian statistics and this results in turn in an enhancement of the diffusion coefficient over its quasilinear prediction. Through energy conservation, a concommitant increase in the growth rate must result as well.

In a preceding paper([6]), two of the authors presented model equations that were proposed in an attempt to take into account the mode-coupling terms which originate in the self-consistency of the electric field, and which invalidate the quasilinear theory in one dimension. This model has received the name of the "turbulent trapping model", since it is devoted to describing those physical effects associated with the partial trapping of the particles in the wave packets.

In the present paper, we numerically study the interaction of a very weak warm beam with a cold and massive bulk plasma, with the aim of detecting the new effects predicted by the turbulent trapping model. Our numerical experiments are simplified as much as possible, but hopefully retain all the basic physics of the process. The most fundamental simplification lies in modelling the bulk plasma as a cold, linear fluid. In effect, it provides nothing more

than the linear dielectric which sustains the electron plasma waves. Apart from a small numerical effect, these are waves with zero group velocity, that is oscillations with stationary envelopes, growing on the energy of the circulating beam particles.

The paper is organized as follows. Section (2) contains a general discussion of the turbulent trapping model, and Section (3) a brief review of previous numerical work. Sections (4-5) are analytic in nature and provide the basic formulation of the problem. In sections (6-8) we continue the analytic work, and review the quantitative predictions of the turbulent trapping model in some detail. It is in sections (9-12) that we embark on the numerical simulations, and present our results for comparison with the analytic work. The discussion of these results is centered on the main predictions of the turbulent-trapping model, concerning the structure of the correlation functions, and the enhancements of the growth rates.

We shall summarize our main conclusions. (1) As regards the correlation functions and the consequent structure of turbulent phase space, the turbulent trapping model provides a surprisingly accurate prediction, especially in view of its semi-qualitative nature. (2) While there is evidence for an enhancement of the growth rates above the quasilinear values, we have not obtained a quantitative verification of the predictions of the turbulent trapping model. In the regime where the model is expected to be strictly valid, the enhancements observed are considerably smaller than predicted; and when the enhancements are closer to what would be expected from the turbulent trapping model, they are observed in a regime where the model is no longer strictly valid. We believe however that these results for the growth rates are not final, and this because our simulations operated under numerical limitations which might be removed in future work.

II. GENERAL DISCUSSION OF THE THEORY.

The non-validity of the quasilinear theory in a regime where the latter was thought to be correct can be understood on a formal basis, starting from the fact that the Vlasov-Poisson equations form a quadratically nonlinear set for the distribution function. Thus the standard techniques, applicable to any quadratically nonlinear equations, can be applied to the Vlasov-Poisson equations as well. These techniques are mainly, the BBGKY hierarchy, the iterative methods used in the Soviet literature in order to derive the Wave Kinetic Equation (with the Random Phase Approximation), and lastly, the Direct Interaction Approximation (DIA). The DIA equations were shown by D. Dubois and M. Espedal([7]), and by others([8]), to add new self-consistency terms (or polarization terms) not present in other renormalized turbulence theories, theories that were based on the simplifying assumption of quasi-Gaussian electric field fluctuations. In fact, such self-consistency terms are easily found to be inherent

in the BBGKY hierarchy and in the iterative methods as well. Moreover, the mode-coupling terms identified by ALP to give a contribution of the same order as quasilinear may be shown to belong to this class of self-consistency terms. The non-validity of the quasilinear theory in the regime $\nu_k > \gamma_k$ is a direct consequence of the self-consistency of the electric field: namely, the statistical properties of the electric field are self-consistently related to the particle motions through the Poisson equation, this self-consistency makes the electric field deviate from Gaussian statistics, and this in turn leads to a modification of the diffusion coefficient in the regime $\nu_k > \gamma_k$. This result has to be contrasted with the so-called stochastic acceleration problem in which the electric field is externally given. In this case the statistical properties of the electric field may be assumed Gaussian, and the quasilinear predictions follow.

A "bootstrap" argument can help to provide a qualitative description of these effects. Let us assume that we start off with a rather particular organization of the turbulent fields, one that partitions them into a set of wave packets of different phase velocities and finite amplitudes, which, for a given phase velocity, have small overlap in real space, and, when considered in velocity space, have barely overlapping trapping widths. In this picture, the envelopes of the wave packets are almost stationary, as the group velocity of the electron-plasma waves is very small. The beam particles stream through these almost immobile packets, to be momentarily trapped and scattered on their way.

If one attempts to partition a turbulent electric field of given total energy and given total spectral width into such a configuration of wave packets, one finds that the characteristic spectral width of each packet is of order $\delta k \approx k(\nu_k/\omega_p)$, where $\nu_k = (k^2 D^{ql})^{1/3}$ is the "classical" resonance broadening frequency([9]) and D^{ql} is the quasilinear diffusion coefficient, proportional to $|E_k|^2$. Each wave packet has a trapping width of order $(D^{ql}/k)^{1/3}$, has a length in real space of order $1/\delta k$, and is such that a particle will reside in it for just about one trapping time, ν_k^{-1}. One can show that such a configuration leads to non-Gaussian statistics of the electric fields.

The fact that the separatrices of the wave packets just barely overlap is essential to our argument. Under such a circumstance, though in most of the phase space near the wave packets particle motion is stochastic, diffusion in a regime so close to the stochasticity threshold need not be quasilinear. Thus, the local diffusion coefficient may differ from the quasilinear one by a factor of order 1([10]). If one then links, through Poisson's equation, the energy loss of the particles to the equal energy gain of the wave packets, one must conclude that at least initially, starting from this particular configuration of wave packets, the electric field energy will grow at a rate γ_k different from the quasilinear. In other words, the motion of an individual particle is sufficiently stochastic to be diffusive over long times, yet is sufficiently coherent over a single trapping time for a modification of the particle's wave emission rate to occur.

Now, two cases can obtain. If the growth rate is larger than the trapping

frequency, $\gamma_k > \nu_k$, the wave packet structure will be destroyed by overlap of neighbors before the modified diffusion and wave emission can occur. In this case, we can conclude that the initial configuration of "barely overlapping" wave packets is irrelevant, because it subsists for a time much shorter than the diffusive time-step. The second case, $\gamma_k < \nu_k$, is the one of interest to us. In this limit, particles are trapped and detrapped many times in one e-folding, and the wave packets can be thought of feeding quasistatically on the nonlinear dynamics of the particles, at a rate different from quasilinear.

The "bootstrap" argument is valid only if we can answer two questions, which apply in the regime $\gamma_k < \nu_k$: (1) how does the wave-packet configuration we have chosen to discuss arise in the first place, and (2) how does it subsist through many e-foldings, when individual wave packets must necessarily disappear, to be replaced by others?

To answer question (1), we can argue that if the modified growth rate regime results in an *enhancement* of the growth rate, $\gamma_k > \gamma_k^{ql}$, then the wave packet structure will eventually dominate any other. This argument, which is valid in the case of a linear instability dominating all other linear waves, is harder to justify in this case because the phenomenon is nonlinear on a microscopic scale. We shall however keep to this qualitative answer.

Question (2) is intimately linked to the self-consistency of the electric field. We have no definite qualitative answer, but can try to rephrase the question in terms of a local energy exchange mechanism. We note that as the wave energy grows, the trapping width of the average wave packet increases. For a constant spectral width, this means that at a given point in space the number of wave packets will diminish with time. This suggests a local mechanism, by which one wave packet can dominate over its neighbors, by diverting the particles on whose energy they would have grown, to the extent of completely depleting some of these neighbors and extending its trapping width to their region of phase space. Assuming this mechanism exists, we have a picture of a configuration slowly transforming itself over a time scale comparable to the growth rate, through a process of competition between neighboring wave packets. Now, such a process is a coupling of modes, between waves differing by $\delta k \approx k(\nu_k/\omega_P)$ and thus, the presence of mode coupling terms in the analytic theory, imposed by self-consistency, is consistent with this picture of a self-sustaining turbulence of wave packets.

Our picture is analogous to the self-sustaining clump turbulence described by Dupree([11]), but with the important difference that in our case the plasma waves display a well-defined dispersion relation $\omega = \omega_k$, imposed by the linear bulk plasma, and which is absent in the formulation of clump turbulence. We shall see that this results in correlation functions of the distribution function which extend over many wave periods, in sharp contrast to the clump correlation function, whose coherence length is limited at most to one wave period. Notwithstanding these differences, and extending the notion of "clump" to the

correlation function in the beam-plasma instability, one might reformulate the wave-packet picture of the preceding paragraphs by saying that the modification of the growth rate, in the clump picture, results from enhanced Cerenkov emission by the clumps, which radiate into a background of adiabatic beam particles (see also Ref.(,[12],[13])).

III. PREVIOUS NUMERICAL WORK.

While simulations of the beam-plasma instability are nothing new (,[14],[15]), performing such simulations under conditions where quasilinear theory can be verified without ambiguity is demanding, both in computational resources and in the care with which the parameters of the simulation must be chosen. This is because behind its apparent simplicity, the weak beam-plasma instability hides several time scales, which must be correctly resolved for quasilinear theory to be applicable (,[16],[17]). The same applies to the turbulent trapping model which assumes constraints similar to those of quasilinear theory.

To our knowledge, the first numerical experiments testing quasilinear theory in its full regime of validity are due to J.C. Adam([18]). These simulations exhibited the formation of discontinuous electric field spectra, ascribed to mode-coupling effects, and showed an enhancement of growth rates over the quasilinear values, but unfortunately were not sufficiently detailed for quantitative conclusions about the turbulent trapping regime to be reached. A set of older and somewhat complementary numerical experiments are those due to A. Bakai and Yu. Sigov ([19]), who emphasized in their study the qualitative observation of phase space structure, without however providing more quantitative descriptions of the phenomena.

In the present work, we have tried to proceed well beyond the results of these previous simulations, by a more systematic measurement of growth rates, by the quantitative description of phase space through the use of correlation functions, and finally, by the direct comparison of numerical results with the analytic predictions of the turbulent trapping model.

IV. PHYSICAL PROBLEM AND APPROXIMATIONS.

The plasma is one-dimensional and consists of one species, electrons moving against an immobile neutralizing background of ions. A sketch of the initial, unperturbed distribution function is shown in Fig.(1).

In our simplified model, the bulk plasma is completely cold and is represented by linear fluid equations for the perturbed bulk velocity and density. The beam plasma on the other hand, is described by the exact Vlasov equation, with no other approximation in the numerical simulations, than those imposed by the finite differencing method we have chosen. This numerical approach,

in which the bulk is "streamlined" so as to simply support linear plasma oscillations, is valid for problems where the detailed beam dynamics are most important. Modelling the bulk as cold and linear then results in a considerable or even vital economy of mesh size.

Let the total, averaged spatial density of the electrons be n_0, with this density split between the bulk, n_{0P}, and the beam, n_{0B}, $n_{0P} + n_{0B} = n_0$. The beam is a small perturbation to the bulk, $n_{0B} \ll n_{0P}$. We model the bulk evolution by the coupled continuity and momentum equations:

$$\frac{\partial}{\partial t}\tilde{n}_P = -n_{0P}\frac{\partial}{\partial x}\tilde{u}_P, \tag{1}$$

$$\frac{\partial}{\partial t}\tilde{u}_P = \frac{q}{m}E(x,t) \tag{2}$$

where $\tilde{n}_P$ and $\tilde{u}_P$ are the linearized fluid variables. The beam is described by a distribution function, $f_B(x,v,t)$ which evolves according to the Vlasov equation:

$$\frac{\partial}{\partial t}f_B + v\frac{\partial}{\partial x}f_B + \frac{q}{m}\frac{\partial}{\partial v}f_B = 0, \tag{3}$$

with the normalization of the unperturbed distribution function:

$$\int_{-\infty}^{\infty} dv\ f_B(v) = n_{0B}, \tag{4}$$

The electric field $E(x,t)$ is determined self-consistently from Poisson's equation:

$$\frac{\partial}{\partial x}E(x,t) = \frac{q}{\epsilon_0}\left[n_{0P} + \tilde{n}_P(x,t) + \int dv f_B(x,v,t) - n_0\right], \tag{5}$$

where we have subtracted from the electron-charge source terms the neutralizing charge of the immobile background ions, qn_0.

We proceed to normalize eqs.(1- 5). We already have a characteristic time-scale, determined by the plasma frequency:

$$\omega_P^2 = \frac{q^2 n_0}{m\epsilon_0}, \tag{6}$$

but, because the bulk is cold, we cannot choose its thermal velocity as a reference velocity, nor the Debye length $\lambda_D \equiv v_T/\omega_P$ as a reference length, as both are zero. Rather, we introduce a reference velocity v_R which is of the order of the beam velocities (Fig.(1)). The reference length is then $\lambda_R \equiv v_R/\omega_P$, and we define the normalized variables as:

$$t' = \omega_P t, \quad x' = x/\lambda_R, \quad v' = v/v_R, \tag{7}$$

$$E' = \frac{qE}{m\omega_P v_R}, \quad u'_P = \tilde{u}_P/v_R, \quad n'_P = \tilde{n}_P/n_{0P}, \tag{8}$$

$$f' = \frac{v_R}{n_{0B}} f_B, \tag{9}$$

Dropping the primes, eqs.(1- 5) then become:

$$\frac{\partial}{\partial t} n_P = -\frac{\partial}{\partial x} u_P, \tag{10}$$

$$\frac{\partial}{\partial t} u_P = E. \tag{11}$$

$$\frac{\partial}{\partial t} f + v \frac{\partial}{\partial x} f + E \frac{\partial}{\partial v} f = 0, \tag{12}$$

$$\frac{\partial}{\partial x} E = R_P \; n_P + R_B \; \left(\int f \; dv - 1 \right). \tag{13}$$

with the normalization:

$$\int dx \int dv f(x, v, t) = L \tag{14}$$

where L is the system length, and where we have defined the parameters,

$$R_B = \frac{n_{0B}}{n_0}, \qquad R_P = \frac{n_{0P}}{n_0} = 1 - R_B, \tag{15}$$

which gauge the relative bulk and beam densities, with $R_B \ll 1$. If $R_B = 0$ exactly, Eqs.(10,11,13) predict linear plasma oscillations, with a plasma frequency $\omega_P = 1$. For convenience, we shall drop all primes in referring to the normalized equations.

For eqs.(10- 13), we can define the normalized energies of the electric field, of the bulk plasma and of the beam plasma particles. These are, respectively:

$$w_E = \frac{1}{2} \int E^2(x, t) \; dx, \tag{16}$$

$$w_P = \frac{1}{2} R_P \int u_P^2(x, t) \; dx, \tag{17}$$

$$w_B = \frac{1}{2} R_B \int \int v^2 f(x, v, t) \; dx \; dv. \tag{18}$$

and with these definitions, conservation of the total energy of the system follows:

$$\frac{d}{dt}w_{\rm tot} = \frac{d}{dt}(w_E + w_P + w_B) = 0, \tag{19}$$

V. LINEAR GROWTH RATES AND QUASILINEAR THEORY.

For a very weak beam, $R_B \ll 1$, eqs.(10- 13) have the dispersion relation:

$$\omega = \pm\omega_k, \quad \omega_k = \mathrm{sgn}(k), \quad |\omega_k| = 1, \tag{20}$$

so that the phase velocities are $v_k = \omega_k/k = \pm 1/|k|$. With this particular definition, the waves on the "+" branch all propagate to the right, and those on the "-" branch all to the left. The linear growth rate of the waves is given by:

$$\gamma_k = R_B \frac{\pi}{2} v_k^2 < f'(v_k) >_s, \tag{21}$$

where $< f(v) >_s$ is the space-averaged distribution function of the beam (see Appendix A for a discussion of ensemble and spatial averages). For the finite-length system of the numerical simulations, the mode structure is discrete, with wave numbers $k = 2\pi n/L$, $n = 1, 2, \ldots$. The electric field has the modal expansion:

$$E(x,t) = \sum_k E_k^+(t) e^{i(kx - \omega_k t)} + \sum_k E_k^-(t) e^{i(kx + \omega_k t)}, \tag{22}$$

where we made explicit right and left-propagating waves. With the beam distribution function confined to positive velocities, only the right-propagating modes $E_k^+(t)$ are resonantly driven by the beam particles, and their amplitudes eventually dominate over the left-going waves $E_k^-(t)$.

The correlation time of the electric fields, defined as the width of the two-point correlation function, is given roughly by:

$$\tau_c \approx \frac{2\pi}{\Delta(\omega_k - kv)} \approx \frac{2\pi}{v\ \Delta k_B}, \tag{23}$$

where Δk_B refers to the total width of the turbulent spectrum excited by the beam. In the usual formulation of quasilinear theory, it is understood that the correlation time is very short, and that we have the ordering:

$$\tau_c \ll \gamma_k^{-1}\ ,\ \tau_{<f>}, \tag{24}$$

where $\tau_{<f>}$ is the characteristic time for the evolution of $< f(v) >_s$. An equivalent way of stating Eq.(24) is through the so-called O'Neil-Malmberg parameter η ([20]), which can be written, with our choice of normalizations:

$$\eta = R_B(v_B/\Delta v_B)^3, \tag{25}$$

In this expression, v_B is the mean phase velocity of the unstable waves. With this definition, the condition $\eta \ll 1$ can be shown to be equivalent to Eq.(24).

If we use the standard formula for the quasilinear diffusion coefficient in the resonant velocity region (see for instance([21])), we find:

$$D^{ql}(v) = \frac{L}{v}\overline{|E^+_{k_v}|^2}, \tag{26}$$

where $k_v = 1/v$ and where L is the total length of the system. The overbar average is defined in Eq.(51) of Appendix A: it is meant to reconcile the statistical properties of a single, long system with those of an ensemble of such systems.

VI. THE EQUATION FOR THE CORRELATION FUNCTION.

The starting point for the turbulent trapping model is the 2-point, 1-time correlation function, which is a measure of the phase-space "graininess" of the beam distribution function. It is defined by:

$$C(x_-, v_-, v_+, t) = < \delta f(x_1, v_1, t)\ \delta f(x_2, v_2, t) >, \tag{27}$$

where $x_- = x_1 - x_2$, $v_- = v_1 - v_2$, $v_+ = (v_1 + v_2)/2$, and where δf is the fluctuation of the distribution function about the averaged distribution, $\delta f = f - < f >$. Implicit in Eq.(27) is the assumption that the turbulence is spatially homogeneous, so that C does not depend on $x_+ = (x_1 + x_2)/2$. Furthermore, C is a slowly-varying function of v_+ (with variation on the scale of the total beam width), so that we shall keep this variable a tacit parameter by writing $C = C(x_-, v_-, t)$ in most places.

On the basis of a number of simplifying assumptions done in the spirit of the turbulent trapping model, one can derive([6]) a Fokker-Planck equation for $C(x_-, v_-, t)$ which has the form:

$$\left(\partial_t + v_-\partial_{x_-} - 2\ (1 - \cos k_+ x_-) D(v_+, t)\partial^2_{v_-}\right) C(x_-, v_-, t) = \\ 2\ \cos k_+ x_-\ D(v_+, t)\left(\partial_{v_+} < f >\right)^2, \tag{28}$$

where $k_+ = 1/v_+$ is the wavenumber resonant with the average velocity v_+. An important feature of Eq.(28) is that the diffusion term $D(v_+,t)$ is left undetermined. It is defined as the one-particle diffusion coefficient, for an ensemble of particles starting at $v(t) = v_+$ and executing a diffusive motion in the turbulent fields until a later time $t' = t + T$. That is:

$$D(v_+,t) =< \left(\frac{\Delta v^2}{2T}\right) >, \tag{29}$$

where $\Delta v = v(t+T) - v(t)$. Provided the time scales are well separated, there will exist a diffusive regime $\tau_c \ll T \ll \gamma_k^{-1}$, such that Eq.(29) provides a value of D independent of T. Now, if quasilinear theory is valid, then from Eq.(29) we must necessarily obtain $D(v_+,t) = D^{ql}(v_+,t)$, where D^{ql} is given by Eq.(26). However, Eq.(28) allows for a more general type of diffusive motion. In fact, the only assumption we retain is that $D(v_+,t)$ grows as the square of the resonant wave amplitude, so that $D(v_+,t) \approx \exp(2\gamma_{k_+}t)$. Because $\gamma_{k_+}^{-1} \lesssim \tau_{<f>}$, this means that the entire right hand side of Eq.(28) has this exponential dependence as well, to within the slow modulation by $(\partial_{v_+} < f >)^2$, which occurs on the $\tau_{<f>}$ time scale. Thus the time derivative on the left hand side of Eq.(28) is of order $\partial_t \approx 2\gamma_{k_+}$.

Let us "freeze" the value of D at a given time, and define an instantaneous trapping frequency and an instantaneous trapping velocity:

$$\nu_{tt} \equiv \left(k_+^2 D(v_+)\right)^{1/3}, \qquad \Delta v_{tt} = \left(D(v_+)/k_+\right)^{1/3}, \tag{30}$$

If we then normalize variables in terms of these trapping parameters:

$$u \equiv v_-/2^{1/3}\Delta v_{tt}, \qquad \xi \equiv k_+ x_-, \qquad \tau \equiv 2^{1/3}\nu_{tt}\, t \tag{31}$$

$$C(x_-,v_-) = \quad 2^{2/3}\Delta v_{tt}^2 \ \left(\partial_{v_+} < f >\right)^2 \ H(\xi,u) \tag{32}$$

we obtain the normalized equation:

$$\left(\delta_\tau + u\partial_\xi - (1-\cos\xi)\partial_u^2 \right) H(\xi,u) = \cos\xi, \tag{33}$$

where $\delta_\tau = O(\gamma_{k_+}/\nu_{tt})$ symbolizes the importance of the time derivative: Eq.(33) is in fact rigorous only provided the time-derivative term δ_τ can be neglected, which requires $\gamma_{k_+} \ll \nu_{tt}$.

Eqs.(28) or (33) incorporate two basic features of the turbulent motion of the beam particles. The first is that as $x_- \to 0$ and $v_- \to 0$, $C(x_-,v_-)$ becomes large, reflecting the fact that particles initially very close in phase space remain correlated for a long time, and do not random-walk independently in velocity space([11]). The second feature of Eq.(28) is that the diffusion coefficients

are periodic in x_-, with a period equal to that of the wave with which the mean velocity of the particles is resonant. Again, this is linked to the fact that particles initially an integral number of wavelengths apart will undergo strongly correlated motion. This second property is only approximate; it will be discussed in more detail in the next section.

VII. SOLUTION IN THE TURBULENT TRAPPING REGIME.

The regime of turbulence is determined by the relative importance, in Eq.(33), of the time-derivative term $\delta_\tau = O(\gamma_{k_+}/\nu_{tt})$. This distinguishes two regimes. In the first, the growth-rate dominates the trapping frequencies, $\gamma^{ql} >> \nu_{tt}$, and in this case we can neglect the $\partial^2_{v_-}$ term in Eq.(28). In effect, the fast growth rate washes out any harmonic strucuture linked to the electric field turbulence (apart from the overall amplitude). G. Laval and D. Pesme([6]) have shown that in this regime one recovers the quasilinear growth-rate.

The "turbulent trapping" regime exists in the opposite limit:

$$\gamma^{ql} << \nu_{tt}, \tag{34}$$

In this limit, we neglect δ_τ in eq.(33), and we can say that the modes grow "quasistatically" when their slow growth is measured on the now relatively short time-scale of the turbulent trapping, ν_{tt}^{-1}. With δ_τ ignorable, Eq.(33) is rigorous and has an exact series solution([6]), given by:

$$H(\xi,u) = \sum_{n=-\infty}^{\infty} H_n(u)\, \exp(in(\xi - \sin\xi)), \tag{35}$$

where the sum excludes the term $n = 0$, and with:

$$H_n(u) = \pi \frac{J_N(N)}{N^{2/3}}\, P(u\, \sigma_n N^{1/3}) \tag{36}$$

with $N = |n|$, $\sigma_n = \mathrm{sgn}(n)$, and with the Airy-related function:

$$P(z) = \frac{1}{\pi}\int_0^\infty \exp\left(-T^3/3 - izT\right)\, dT \tag{37}$$

Graphs of $H(\xi,u)$, obtained from the analytic series (35), are shown in figs.(2). A salient property of this approximate solution is that $H(\xi,u)$ has a logarithmic divergence as $\xi, u \to 0$, with the asymptotic expression:

$$H(\xi,u) \approx \frac{1}{2^{1/3}} \log \frac{3}{(\xi^2 - 2^{2/3}\xi u + 2^{1/3}u^2)}, \tag{38}$$

This divergence reflects the property required of Eq.(28), that points of phase space initially very close remain correlated for long times. A similar structure arises in the solution of T.H.Dupree's equations for turbulence in a bulk plasma([11]).

The series solution, Eq.(35), diverges as $\xi, u \rightarrow 0$ because we have neglected the δ_τ term in Eq.(33), a term reflecting the importance of the time derivative in Eq.(28) for small separations x_- and v_-. Indeed, we expect (35) to break down when the terms $u\partial_\xi$ and $(1-\cos\xi)\partial_u^2$ in Eq.(33) are comparable to δ_τ. If we assume that $\partial_\xi \approx \partial_u \approx 1$, in the normalized, approximate solution $H(\xi, u)$, then the δ_τ term becomes important when $u \leq \delta_\tau$ and $\xi \leq \delta_\tau^{1/2}$. In physical units, the conditions for the validity of (35) are then $|v_-| \gg \gamma_{k_+}/k_+$ and $|k_+ x_-| \gg (\gamma_{k_+}/\nu_{tt})^{1/2}$.

While an analytic solution with $\partial_t \neq 0$ has not been found, we can obtain the special value of $C(0,0)$ very simply, by letting $x_-, v_- \rightarrow 0$ in Eq.(28), which eliminates all but the first term on the left. We have, with $\partial_t = 2\gamma_{k_+}$:

$$C(0,0) = <(\delta f)^2> = \frac{D(v_+)}{\gamma_{k_+}} \left(\partial_{v_+} < f >\right)^2, \tag{39}$$

an expression which assumes that $\gamma_{k_+}^{-1} \ll \tau_{<f>}$.

We should also stress that the strict periodicity of $C(x_-, v_-)$ as a function of x_- is an approximation which results from assuming that particles at $v = v_+$ feel the single wave number $k = k_+ = 1/v_+$. To be consistent with the spirit of the turbulent trapping model, we must in fact assume that the particles see an entire wave packet, still centered about k_+, but of width $\delta k_{tt} = k_+ \nu_{tt}$. The maximum correlation length, l_{tt}, will be of the order of the length of this wave packet:

$$l_{tt} = 1/k_+ \nu_{tt} = 1/k_+^{5/3} D^{1/3}, \tag{40}$$

Qualitatively, we expect the series solution (35) to be modified by an envelope function of width l_{tt}, such that successive peaks of $C(x_-, v_-)$ diminish in amplitude, tending to zero for $|x_-| \gg l_{tt}$. As we shall see, this behavior is numerically confirmed.

By inspection of Fig.(2a), we can see that the total width of the profile of $H(u,0)$ is about 3. This width in v_- is then approximately $3 \times 2^{1/3}\ \Delta v_{tt} \approx 4\Delta v_{tt}$. Now, for Eq.(28) to be valid, the width in v_- of the correlation function must be small compared to the beam width. This imposes the reasonable trapping width constraint:

$$4\Delta v_{tt} \ll \Delta v_B, \tag{41}$$

where Δv_B is the beam width over which waves are excited. In other words, any turbulent structure must remain small, and it is in this sense that the turbulent trapping model remains within weak turbulence theory.

VIII. ANALYTIC GROWTH RATES IN THE TURBULENT TRAPPING REGIME.

By using Poisson's equation, we can express the growth rate γ_k in terms of a velocity integral of the correlation function. G. Laval and D. Pesme([6]) have used this expression to find the growth rate in the turbulent trapping regime, by what might be termed a "bootstrap" method. First, $C(x_-, v_-)$ is derived from the series solution in Eq.(35). With Poisson's equation, this results in an expression where γ_k is an explicit function of D, the undetermined diffusion coefficient. It is then found that by choosing a particular form for γ_k and D, global energy conservation is satisfied while the functional relation between γ_k and D remains true. The expressions for γ_k and D are simply:

$$\gamma_k = 2.2\ \gamma_k^{ql}, \tag{42}$$

$$D(v) = 2.2\ D^{ql}(v), \tag{43}$$

where γ_k^{ql} and $D^{ql}(v)$ are given by eqs.(21) and (26). The numerical factor of 2.2 comes from the summing of a series of harmonics in Eq.(35), in the form of a series of Bessel functions. The striking feature of eqs.(42,43) is that the enhancement of the growth rate and diffusion coefficient is this simple numerical factor, independent of k and of the level of turbulence, provided $\nu_{tt} \gg \gamma_k$.

Analytic work([4]), done in the complementary regime $\nu_{tt} < \gamma_k$, suggests a refined threshold for turbulent trapping, with the strong inequality replaced by the condition:

$$\nu_{tt} \geq 5\ \gamma_k, \tag{44}$$

The work of Ref.([4]) also suggests that, starting from initial conditions, the enhancement of the growth rate in the turbulent trapping regime will occur only after a substantial time lapse, that is after at least a few e-foldings of the electric field. This is because for eqs.(42,43) to be valid, the non-resonant harmonics of the Fourier components of the electric field must be in a quasistatic equilibrium with the fundamental, resonant harmonics. At $t = 0$, the nonresonant components are rigorously zero, and thus a finite time must elapse, before the mode-coupling mechanisms can build-up the hierarchy of modes, mutually scattering into each other, which contribute to the enhancement of the growth

of the fundamental. If N is the number of e-foldings undergone by the electric field, we shall require:

$$N \approx 3 - 5, \tag{45}$$

for a regime of enhanced growth rates to manifest itself.

IX. THE NUMERICAL SCHEME.

The Vlasov solver for Eq.(10) uses a finite difference scheme developped by J.P. Boris and D.L. Book([22]) , the so-called "flux-corrected transport" method, which exhibits a particularly low diffusivity, while maintaining good numerical stability even with very sharp density profiles in phase space. This scheme is combined with a split-step method devised by C.Z. Cheng and G. Knorr([23]), in which transport of the distribution function alternatively proceeds in x and in v.

The distribution function for the beam particles, $f(x,v)$, is defined on a mesh with N_x points in the spatial dimension x and N_v points in velocity v, with spacings Δx and Δv respectively. The total system length is $L = N_x \Delta x$, with boundaries in x at $x_{min} = 0$, $x_{max} = L$. The boundaries in velocity are at $v = v_{min}$ and $v = v_{max}$. The spatial boundary conditions are periodic, while at $v = v_{min}, v_{max}$ we impose $f = 0$, a good approximation provided f is already very small some distance from the velocity boundaries. We advance the system in time with a time-step Δt, usually chosen so that $\omega_P \Delta t = 0.2$.

The bulk equations are solved independently on the one-dimensional spatial mesh, using fast Fourier transforms in a leapfrog scheme. Beam and bulk equations are then coupled through Poisson's equation, also solved with Fourier transforms.

Because our simulations are aimed at exploring the initial turbulence created in the beam-plasma instability, we think of the beam distribution function as a tunable source of free energy, and we define its shape to obtain a constant initial growth rate([19]) over a large band of phase velocities(figs.(3a,b)). This is done by piecing together simple functions of velocity (see Appendix C). Our choice of an initial distribution function is somewhat artificial, but it has the great advantage of avoiding trapping effects which arise from the early dominance of a single mode.

In Table I, we list the principal parameters of the two simulations to which we shall refer in the following sections. In the table, we indicate how well the validity conditions, summarized by eqs.(54-58) of appendix B, are satisfied.

We initially perturbed the beam distribution function and the bulk plasma density with a purely spatial modulation, so as to obtain an initial electric field:

$$E(x,0) = \sum_{k=k_1}^{k_2} e_k \sin(kx + \phi_k), \tag{46}$$

where the phases ϕ_k are chosen randomly from one mode to the next, and where the coefficients e_k are defined so as to provide an electric field with a given, smooth amplitude spectrum. The modes in $k_1 \leq k \leq k_2$ are restricted to lie in the unstable part of the spectrum. (Fig.(3a)).

The initial standing wave of Eq.(46) splits into right-propagating and left-propagating waves, with only the former amplified by the beam-plasma interaction. Neglecting ballistic effects, from Eq.(22) we have the linear behavior:

$$E(x,t) = \frac{1}{2} \sum_{k=k_1}^{k_2} e_k \left[\sin(kx - t + \phi_k)e^{\gamma_k t} + \sin(kx + t + \phi_k)\right], \tag{47}$$

XI. THE NUMERICAL CORRELATION FUNCTION.

In this section, we consider the numerical results obtained in Simulation 1 (Table I), for the correlation functions of the beam distribution function. The initial distribution function used in the simulation, the resulting linear growth rates and the phase velocities of the modes initially excited are shown in figs.(3). The initial growth rate was $\gamma_L = 2.19 \times 10^{-3}$ (obtained with a relative beam density $R_B = n_B/n_0 = 2 \times 10^{-3}$), and the modes were excited in the range of phase velocities $1.15 \leq v_k \leq 2.55$ (79 modes in $0.392 \leq k \leq 0.871$). For the form of the initial excitation, we chose a nonuniform distribution of mode amplitudes, with the dependence on wave number $e_k \approx 1/k^3$. This choice insured that the same amount of resonance overlap obtained for all modes of the spectrum. The additional advantage of this uneven distribution of amplitudes is that it permitted us, at any one instant in time, to measure the correlation function for an entire range of trapping widths Δv_{tt}, by scanning $v = v_+$ across the width of the beam.

If we consider a mode in the center of the spectrum, say with $v_k = 1.75$ ($k = 0.564$), we find that initially $\nu_{tt}/\gamma_L \approx 4.5$, and at the end of the simulation $\nu_{tt}/\gamma_L \approx 9$. Thus according to Eq.(44) the center of the spectrum was in the turbulent trapping regime from the very onset of the instability. However, Simulation 1 proceeded for only about one e-folding, to $t = 500$, an evolution time which is probably insufficient for the manifestation of enhanced growth rates (Eq.(45)). The discussion of the latter effects is deferred to the next sections, where we discuss them in relation to a longer simulation (3.2 e-foldings).

The evolution of the total field energy $w_E(t)$ is shown in Fig.(4). The oscillating character of $w_E(t)$ comes from the interference of the growing right-propagating waves with the left-propagating waves of constant amplitude.

The final space-averaged distribution function,$< f(v) >_s$, is shown in Fig.(5), where it is compared on the same graph to the initial distribution function. It can be seen from this figure that little modification of $< f(v) >_s$ has occured, indicating that at this point $\tau_{<f>} > \gamma^{-1}$. By looking at a cross section of f at fixed x, as is done in fig(6), we can also see that the amplitude of fluctuations in the non-averaged distribution function has remained small.

So that we may obtain a more general view of the phase space organization of the beam, in Fig.(7) we show the contour lines of the final distribution function, $f(x,v)$ at $t = 500$, for the entire length of the simulation, $0 \leq x \leq 1024$. We shall now interpret this figure. We first note that at $t = 500$, the wave spectrum has remained almost entirely confined to the initial range of phase velocities, $1.15 \leq v_k \leq 2.55$. Thus we expect trapping to occur within this velocity range, and the motion of particles to be adiabatic beyond it, with however some extension of the trapping region above and below the range of excited phase velocities, due to the finite trapping widths of the waves. This is indeed suggested by the contours of Fig.(7). For $v > 2.8$, the distribution function is only slightly perturbed by the wave turbulence, while in the resonant or near-resonant range $2.8 \geq v \geq 1.1$ the contours display a "graininess", consisting of closed or almost closed patterns or "grains", suggestive of the formation of small plateaus in the distribution function. When they are examined individually, these patterns have dimensions in x and v which qualitatively scale as expected. At large velocities (say $v = 2.3$), where the resonant wave amplitudes are large ($4\Delta v_{tt} = 0.24$), the circles or semicircles of the contours are wide in velocity. At low velocities (say $v = 1.3$), the resonant wave amplitudes are small ($4\Delta v_{tt} = 0.15$) and so is the size of the "grains". The spatial arrangement of the "grains" also reflects the properties of the resonant wave: one can verify that they have a spacing roughly equal to the wavelength of the wave, which is $\lambda_+ = 2\pi/k_+ = 2\pi v_+$.

To further clarify these observations, we show in Fig.(8) a perspective plot of a small portion of the distribution function, extracted from the region which is labelled "Area 1" in Fig.(7). This picture displays the plateaus, which were suggested by the contour plot in Fig.(7), in a more convincing manner, and it is from these plateaus that we infer the existence of locally trapped particles. A striking feature of the figure is that phase space appears very regular when it is seen on this small scale, a central prediction of Eq.(28). As noted above in Section 5, this regularity is only approximate, and should break down beyond the length of a resonant wave packet, a length which we estimated to be of order $l_{tt} = 1/k_+\nu_{tt}$(Eq.(40)). For the "reference" velocity $v_+ = 1.75$, this length is $l_{tt} \approx 90$ at the end of the simulation. In Fig.(9) we blow up the longer region which is labelled "Area 2" in Fig.(7), and display it in perspective. This picture extends over a length in x of 160 units, almost three times the length of Area 1. The figure shows that when seen over this larger space scale, the alignement of successive plateaus loses its regularity, indeed over a length which is comparable

to $l_{tt} \approx 90$.

The discussion given above is qualitative and visual in nature. To probe the structure of Fig.(7) in a quantitative manner, we need a more exact numerical tool, and such a tool is precisely the correlation function of Eq.(27). In the simulation, we evaluated $C(x_-, v_-)$ by performing a spatial average over the length of the system. Thus, for given values of $x_- = i_-\Delta x$, $v_- = j_-\Delta v$ and $v_+ = v_{min} + (j_+ - 1)\Delta v$, we calculated the sum:

$$C(x_-, v_-, v_+) = \frac{1}{N_x} \sum_{i=1}^{N_x} f_{i,j_+} \cdot f_{i+i_-,j_++j_-}, \tag{48}$$

where $f_{i,j}$ is the distribution function at the mesh point (i, j).

To make the link with the analytic solution given by Eq.(35), we needed to know the value of the diffusion coefficient in eqs.(30). The simplest approach was to assume that $D = D^{ql}$ and obtain D^{ql} from Eq.(26). In so doing, we ignore any possible increase in diffusion, as would be indicated by Eq.(42). This is justified to the extent that, as mentioned above, we do not expect the system to have had the time develop enhanced diffusivity within a single e-folding. Furthermore, should D be enhanced by the amount suggested by Eq.(42), this enhancement will lead to a quite modest broadening of the trapping width, with $\Delta v_{tt} = (D/k)^{1/3} = 1.3\Delta v_{tt}^{ql}$. From the discussion that follows, it will be seen that the observation of such a moderate broadening is difficult to obtain from the inspection of the numerical correlation function. Thus, a less ambiguous detection of enhancement is to be obtained from the direct measurements of the growth rates, to be presented in the next section.

We first consider the structure of the correlation function in velocity space, by plotting $C(0, v_-)$, for a fixed value of the mean velocity v_+. Thus in Fig.(10), we compare the numerical results for $C(0, v_-)$ with the predictions of the series solution, Eq.(35), for the mean velocity $v_+ = 1.745(\Delta v_{tt} = 0.034)$. We noted above that the series solution blows up at $v_- = 0$, and is not valid for $|v_-| \ll \Delta v_{tt}$. However, in the region where the analytic solution is valid, that is for $|v_-| \gg \gamma_{k_+}/k_+ \approx 0.0035$, the numerical and analytic curves are in qualitative agreement, in that their central peaks have almost the same width, and that both correlation functions are small when $|v_-| \gg 2\Delta v_{tt}$. This confirms the importance of the quantity Δv_{tt} as the basic turbulent velocity scale. We have further analysed the agreement between the two curves of Fig.(10) by plotting in Fig.(11) the width δv_{tt} of the central peak of the correlation functions, now as a function of the parameter v_+, with v_+ varying across almost the entire range of phase velocities. The width of the central peak is defined as the separation between the two zeros at the base, and is given analytically by $\delta v_{tt} = 4.32\Delta v_{tt}$. The agreement remains rough, but reflects the correct dependence on the resonant field amplitudes.

While the analytic $C(0,v_-)$ strictly falls to zero for $|v_-| \gg \Delta v_{tt}$, the numerical correlation function in Fig.(10) retains sizeable fluctuations. We suspect that this results from the finite length of the simulation ($L = 1024$), which limits the number of uncorrelated regions contributing to the spatial average which defines the correlation function. For $v_+ = 1.745$, the correlation length is roughly $l_{tt} \approx 90$, and thus in the neighborhood of this velocity only about $L/l_{tt} \approx 10$ statistically independent regions exist in the system. The fluctuations in Fig.(10) are then the noise which results from doing statistics with only about 10 samples. We suspect that this noise could be reduced by additional numerical processing, in which the correlation function, obtained as a "snapshot" from Eq.(48), would be further averaged in time, over a period of at least a few trapping times ν_{tt}^{-1}. However, we have not attempted to implement such a scheme.

While we do not have an analytic solution for $C(0,v_-)$ in any finite range of $|v_-| \ll \Delta v_{tt}$ about $v_- = 0$, we did find an expression for the single peak value $C(0,0)$, Eq.(39). In Fig.(12), we plot as a function of v_+ the numerical and analytical values obtained for $C(0,0)$. This graph indicates that Eq.(39) is indeed qualitatively correct, but that a sizeable quantitative difference exists between the analytic prediction of $C(0,0)$ and the numerical result. We should note that the numerical value of $C(0,0)$ is relatively insensitive to changes in grid size (a 20% change results upon halving Δx or Δv), a result which gives us confidence that the differences observed in Fig.(39) are not due to spurious numerical effects. We suspect that the finite rate of change of the average distribution function, which is not much smaller than the growth rate (with the estimate $\tau_{<f>} \approx 2000 \approx 4 \times \gamma_{k_+}^{-1}$), might be responsible for reducing the value of $C(0,0)$ to under what would be expected from the uncorrelating effect of γ_{k_+} alone.

We next consider the spatial structure of the correlation function, by plotting $C(x_-,0)$, once again for fixed v_+. In Fig.(13) this is done for $v_+ = 1.745$, over the range $-50 \leq x_- \leq 50$. The curve of $C(x_-,0)$ displays the two main features predicted by the analytic theory. The first feature is a relatively fast and almost periodic dependence on x_-, with a period we label L_{pp} ("peak to peak"). The second feature is a broad envelope, of width we label L_m, which modulates the fast dependence of the correlation function. In what follows, L_m is defined graphically, as the length over which the envelope decays to $1/e$ of its peak value, and is estimated by linear extrapolation from the first three central peaks of the correlation function. According to the analytic results, we should have $L_{pp} = 2\pi/k_+$ and $L_m \approx l_{tt}$ (eqs.(40)). The agreement is shown in figs.(14,15). It is very good for L_{pp} and at least qualitatively correct for L_m. We should stress however that the result $L_m \approx l_{tt}$ was derived from very qualitative considerations; thus the intersection of some parts of Fig.(15) should be regarded as a coincidence.

In Fig.(16), we plot the numerical $C(x_-,0)$ for a smaller range of x_- than in

Fig.(13), $-12 \leq x_- \leq 12$, and make a direct comparison with the series solution, Eq.(35). We note once again that the analytic solution unfortunately artificially blows up at $x_- = 0$ (and at multiples of the period $2\pi/k_+$). Notwithstanding this, qualitative agreement for values of x_- not too close to these points is good.

XII. THE NUMERICAL GROWTH RATES.

In this section we consider the numerical results for the growth rates which were obtained in Simulation 2 (Table I) by the direct measurement of the field amplitudes. This simulation was run with the hope of observing a significant enhancement of the growth rates over the quasilinear values, and in this it differs from Simulation 1 in two important respects: the initial amplitude spectrum $|E_k|$ was chosen uniform in k, as opposed to $|E_k| \approx 1/k^3$ previously, so as to minimize nonuniformity in trapping widths, and the system was left to evolve over a significantly longer time, that is for about 3.2 e-foldings of the electric field amplitudes. As noted above (Eq.(45)), several e-foldings should be necessary for the equilibration of the nonresonant harmonics to occur, and hence for the regime of enhanced growth rates to set in. The initial linear growth rate was $\gamma_L = 1.2\ 10^{-3}$ (obtained with a beam density of $R_B = n_B/n_0 = 7.4\ 10^{-4}$) and the waves were initially excited in the range of phase velocities $0.668 \leq v_k \leq 1.81$ (77 modes excited in $0.552 \leq k \leq 1.497$). For the waves near the central value of phase velocity $v_k = 1.0$, we initially had $\nu_{tt}/\gamma_k = 5.8$, and at the end of the run, $\nu_{tt}/\gamma_L = 150$, so that as in the previous simulation, the evolution of these waves was in the turbulent trapping regime from the very outset of the instability.

We ran Simulation 2 for $\omega_p T = 2875$ time units (about 450 plasma periods), during which the total electric field energy increased about 210-fold. In Fig.(17) we show the amplitude spectrum of the forward waves, $|E_k^+|$ at $t = 0$ and at the final time $t = 2875$, that is after about 3.2 e-foldings of the field amplitudes. The spectrum at $t = 2875$ displays two distinctive features. The first is that the average spectrum, which started out as rigorously flat, has undergone nonuniform amplification, with a peak toward the lower values of k, near $k = 0.8$. The Fourier amplitudes for $k > 0.8$ have not grown as much, and there has been little growth at the very edges of the spectrum. This nonuniformity can be ascribed to the concurrent flattening of the average distribution function (Fig.(18)), which is becoming severe towards the end of the simulation. This flattening, when weighted with the factor of v_k^2 in Eq.(21), has a more pronounced effect on the growth rate of the waves with lower phase velocities (and hence for the waves with larger k).

The second distinctive feature of Fig.(17) is the jagged aspect of the small-scale structure of the spectrum. There are large and irregular amplitude variations from one mode to the next, and this results in the spikes which can be seen in Fig.(17). We believe that this irregular spectrum, which was also

observed by J.C.Adam ([18]), is due to the evolution of the system into a set of uncorrelated subsystems, each of characteristic length l_{tt}. Each Fourier mode can then be written as a sum of independent random variables([24]), with, as a consequence, the statistical independence of neighboring modes.

To give statistical meaning, in terms of ensemble averages, to the mode amplitudes obtained in Simulation 2, we used the convolution average defined in Eq.(51) to calculate $\overline{|E_k|^2}$. We then numerically computed the average growth rate according to:

$$\overline{\gamma}_k = \frac{1}{2}\frac{\partial}{\partial t}\log \overline{\left|E_k^+(t)\right|^2}, \tag{49}$$

which is a definition of γ_k equivalent to the one assumed in Eq.(42). We compared this to the growth-rate predicted by quasilinear theory, Eq.(21), using the numerical, space averaged distribution function which is obtained from the simulation:

$$\gamma_k^{ql} \equiv R_B \frac{\pi}{2} v_k^2 < f'(v_k,t) >_s, \tag{50}$$

As a function of velocity, the numerical quantity $< f'(v) >_s$ displays short-scale fluctuations which are probably the result of the relatively short length of the simulation, as compared to the correlation length ($L/l_{tt} \approx 10$). To reduce these fluctuations, we resorted to additional smoothing of $< f'(v) >_s$, by averaging its value over neighboring points in velocity, through convolution with a triangular window $W(v)$ of the same form as the one used in Eq.(51). While we used the same averaging function W for $< f(v) >_s$ and $|E_k|^2$, we should note that the statistical operations involved are essentially independent.

In Fig.(19), we show the evolution of $\gamma_k^{ql}(t)$, for $k = 1.0$, $v_k = 1.0$. The considerable variation of γ_k^{ql} over the time scale $0 \leq t \leq 2875$ is consistent with the large modification of $< f(v) >_s$ which can be observed in Fig.(18), where we compared the initial and the final average distribution functions. It is apparent from this latter picture that we are running into a regime where $\tau_{<f>} < \gamma_k^{-1}$. This is a result of the long running time of the simulation, and indirectly of the constraints placed on the initial field amplitudes, which cannot be infinitesimal, but have to be sufficiently large for the condition $\nu_{tt}/\gamma_k > 5$ to be satisfied at $t = 0$.

Thus, inspection of Fig.(19) indicates that for $t > 1000$ the characteristic time $\tau_{<f>}$ for a change of order unity to occur in $< f'(v,t) >_s$ is of order $\tau_{<f>} \approx 1300$, comparable to or smaller than the e-folding time of the electric field, which is initially $\gamma_k^{-1}(0) = 830$, and which decreases to $\gamma_k^{-1} \approx 2000$ towards the end of the simulation. We may conclude that the present simulation is not an ideal verification of behavior in the turbulent-trapping regime, which assumes $\gamma_k^{-1} \lesssim \tau_{<f>}$.

The evolution in time of the ratio $\overline{\gamma}_k/\gamma_k^{ql}$ for $k = 1$ is plotted in Fig.(20). The distinctive feature of Fig.(20) is that $\overline{\gamma}_k/\gamma_k^{ql} > 1$ throughout the evolution of the system. A further observation is that the ratio $\overline{\gamma}_k/\gamma_k^{ql}$ is not constant, but undergoes a slow increase, reaching a value of about 1.2 after 2.6 e-foldings of the electric field, at $t = 2000$. In the final time interval, $2000 \leq t \leq 2875$, $\overline{\gamma}_k/\gamma_k^{ql}$ undergoes a sharper rise reaching a maximum value of 1.6.

It is tempting to explain the enhancement of $\overline{\gamma}_k/\gamma_k^{ql}$ to values greater than 1 by the effects predicted by ALP and described by the turbulent-trapping model. However, we must note that the enhancement of the growth rate remains modest during most of the simulation, with $\overline{\gamma}_k/\gamma_k^{ql} \leq 1.2$ during the first 2.6 e-foldings of the electric fields. This enhancement is well short of the value of 2.2 predicted by the turbulent trapping model, Eq.(42). Furthermore, when $\overline{\gamma}_k/\gamma_k^{ql}$ increases to a more sizeable value (from 1.2 to 1.6, in the time interval $2000 \leq t \leq 2875$), it does so precisely in a regime where the trapping widths have become quite large, that is where neither quasilinear theory nor the turbulent trapping model are expected to be strictly valid in the first place.

The correlation of large trapping widths with strong enhancement of the growth rates is made clearer if we look at "snapshots" of the ratio $\overline{\gamma}_k/\gamma_k^{ql}$, plotted now as a function of k. This is done in figs.(21,22), for the fixed times $t = 2000$ and $t = 2875$. In the figures, we have indicated the interval in k corresponding to the turbulent trapping width $4\Delta v_{tt}$, for waves resonant with $v_k = 1.0$. Thus, at the end of the simulation (Fig.(22)), the large enhancement of the growth rate occurs when the trapping width is itself large, with $4\Delta v_{tt}/\Delta v_B \approx 0.3$. Furthermore, this enhancement is accompanied by strong edge effects, so that $\overline{\gamma}_k/\gamma_k^{ql}$ is more strongly nonuniform in k as well (similar nonuniform profiles were observed by J.C. Adam([18])). This strong nonuniformity can be ascribed to the fact that in this regime, the waves derive their energy from large populations of trapped particles, which are trapped in only a few wave packets within the entire beam. The local slope $< f'(v) >_s$, which defines the quasilinear growth rate, is no longer the salient physical parameter responsible for the growth rate of the resonant waves. In this extreme regime, it is not surprising that the growth rates are uneven, on account of the few wave packets exchanging energy with the particles, and that they are quite different from the quasilinear growth rates.

However, Figs:(20- 22), have a striking characteristic which moves us to interpret the increase of growth rates as resulting from effects in the spirit of those predicted by ALP. While the nonuniformity in the growth rate observed in Fig.(22) can be ascribed to the large trapping widths of the wave packets, this situation does not by itself account for the fact that the growth rates are greater than quasilinear, *everywhere* across the spectrum.

Furthermore, the finite resolution of the grid severely limits the number of nonresonant harmonics which can be generated by the partially trapped

particles. Thus, the maximum physical wave number k allowed on the mesh is of order $\pi/2\Delta x \approx 3$, so that the waves with $k \approx 1$ may interact at most with 3 harmonics. The result of this truncation may be a significantly smaller enhancement of the growth rate than predicted by Eq.(42), which assumes that an infinite cascade of harmonics contibutes to the enhancement. Thus, we suspect that this may explain the low enhancements observed in Fig.(21).

XIV. CONCLUSION.

We performed numerical simulations to verify the existence of a new turbulent regime in the development of the weak beam-plasma instability, and more specifically, to validate the predictions of the "turbulent-trapping" model concerning correlation functions and enhanced growth rates.

Our most definitive conclusions regard the predictions of the turbulent trapping model for structure in phase-space. Both qualitatively and quantitatively, this model provides good predictions for the correlation functions of the beam distribution function. This important result supports the qualitative picture in which the turbulence is composed of wave packets whose trapping domains barely overlap in phase space, with a characteristic width in velocity $\Delta v_{tt} = (D/k)^{1/3}$, and a correlation length in space of $l_{tt} = 1/k^{5/3}D^{1/3}$, with $D \approx D^{ql}$.

Less definitive are our conclusions regarding the prediction of an enhancement of the growth rates, an enhancement which might otherwise be expected on the basis of the success of the model in predicting the correlation functions. The enhancements which are observed are modest (enhancements of 1.2-1.6, compared to a prediction of 2.2), with upper values occuring in a regime of marginal validity for the quantitative predictions of the model. However, we suspect that the nonideal aspects of the simulations are responsible for some reduction of the numerical growth rates which were observed. Thus, we conclude that there is nonetheless qualitative evidence for enhanced growth rates.

Future work might bear on more ambitious simulations, which can overcome the numerical limitations of the present ones, which suffered from a relatively coarse numerical mesh. Another approach in the study of the effects of trapping on the growth rates would be to shift the emphasis from weak turbulence, to the study of what might be called "moderate" turbulence (a few wave packets in the width of the beam), a regime in which the choice of numerical parameters is less delicate. The insights gained from studying this regime of more vigorous trubulence might then be extrapolated back to the weaker regime assumed by the ALP model.

Acknowledgements.

The authors wish to thank Dr. J.C. Adam for suggesting the numerical approach taken in this work. Computation was done at the Ecole Polytechnique, Palaiseau, France, and at the National Magnetic Fusion Energy Computing Center, Livermore, California. Dr. K. Theilhaber was funded on ONR contract N00014-85-K-0809 and DOE contract FG03-86ER53220.

APPENDIX A: ENSEMBLE AVERAGES VS. SPATIAL AVERAGES.

Statistical theories of turbulence usually are stated in terms of the ensemble averages of spectral quantities. Thus one might conclude that the proper numerical study of turbulence would require performing a large number of numerical simulations, each with different initial conditions, and averaging the final results. In fact, if the turbulence studied is homogeneous in space, in principle all the relevant information about ensemble averages can be extracted from any one realization in the ensemble, that is from a single numerical simulation, provided that the system is long enough. The criterion for sufficient length is that the length L of the system be much longer than the correlation length l_c of the quantity investigated(see ([25]) for equivalent discussions of data processing, for power spectra in the time and frequency domain).

For instance consider the squared Fourier amplitude of the electric field, which will be the main spectral quantity of interest. The problem is to approximate its ensemble average, which we denote by $< |E_k|^2 >$, from the results of a single simulation. The prescription is as follows: we first obtain the "raw" squared Fourier spectrum $|E_k|^2$, directly from the numerical $E(x)$ resulting from a single computer run. In general, this quantity will be a rather chaotic function of k. We then perform a convolution to define the smoothed average:

$$\overline{|E_k|^2} \equiv \sum_K W(K-k)\,|E_K|^2, \tag{51}$$

where $W(K)$ is a window function such that $\sum_K W(K) = 1$. In what follows, we choose $W(K)$ to be triangular in shape, with $W(K) = (\Delta k/k_w)(1-|K|/k_w)$ and $W(K) = 0$ for $|K| \geq k_w$. Provided that the width of $W(K)$ is small compared to the total spectral width (that is, the inverse correlation length), but large compared to the mode spacing ($k_w \gg \Delta k = 2\pi/L$), Eq.(51) will provide an approximation to the ensemble average, $\overline{|E_k|^2} \approx < |E_k|^2 >$.

In dealing with spatial quantities, such as the spatial correlation functions or the average distribution function, it is legitimate to replace the ensemble average by a sliding spatial average over the entire length of the system, provided once again that the system is long compared to the correlation length. In what follows we adopt the following conventions: the unadorned angle brackets $< \ldots >$ refer to ensemble averages, the addition of a subscript "s" denotes a spatial average, $< \ldots >_s$, and the overbar notation will be reserved for the spectral quantities, to denote the filtering operation of Eq.(51).

APPENDIX B: CONDITIONS OF VALIDITY.

In this Appendix we summarize the several conditions which define the turbulent trapping regime. In addition to those stated in the main text, a condition on the validity of the derivation of (42,43) is that dispersion within a turbulent wave packet is small over a time scale of $1/\gamma_k$. This is expressed by the condition([4]):

$$\left|\frac{\partial^2\omega_k}{\partial k^2}\right| \left(\frac{\nu_{tt}}{|v_k - v_{gk}|}\right)^2 \ll \gamma_k, \tag{52}$$

where v_k is the phase velocity and v_{gk} the group velocity of the waves. The cold bulk plasma is theoretically dispersionless, but in fact has the numerical dispersion relation $\omega_k = 1 - k^2\Delta x^2/8$ valid for $k\Delta x \ll 1$. With $v_k \approx 1/k$, $|v_{gk}| = |\partial\omega_k/\partial k| \ll v_k$, Eq.(52) reduces to:

$$\delta_{disp} \equiv \frac{1}{4}\frac{k^2\Delta x^2\nu_{tt}^2}{\gamma_k} \ll 1, \tag{53}$$

This constraint is necessary, in addition to those already outlined, for a valid test of the turbulent trapping theory.

To summarize all constraints, we have (eqs.(24),(41),(44) and (53), and the paragraph following Eq.(44)):

$$\tau_c \ll \nu_{tt}^{-1} \ll \gamma_k^{-1} \lesssim \tau_{<f>}, \tag{54}$$

$$4\Delta v_{tt} \ll \Delta v_B, \tag{55}$$

$$\nu_{tt} \geq 5\ \gamma_k, \tag{56}$$

$$\delta_{disp} = \frac{1}{4}\frac{k^2\Delta x^2\nu_{tt}^2}{\gamma_k} \ll 1, \tag{57}$$

$$N \approx 3 - 5, \tag{58}$$

where N is the number of e-foldings during the evolution of the instability. Eqs.(54,55) are general conditions for weak turbulence, and are required for quasilinear theory as well. Only eqs.(56,57,58) specifically define the turbulent trapping regime.

Eqs.(55), (56) and (58) are the most stringent conditions imposed on the simulations. For instance, suppose that we want to follow the evolution of the system through N e-foldings of the field amplitudes, while remaining in the

turbulent trapping regime throughout the computer run. For a fixed beam width, Eq.(55) limits the amplitude of the final electric field. This implies that the initial field amplitudes have to be scaled-down by a factor of order e^{-N} from a rigid, fixed upper limit. Thus the initial value of $\nu_{tt} \approx |E|^{2/3} \approx e^{-2N/3}$ is small. In turn, Eq.(56) implies that the initial growth rate must be sufficiently small as well, with the same scaling $\gamma \approx \nu_{tt}/5 \approx e^{-2N/3}$. Thus the total run time T of the simulation, which,according to Eq.(58), has to undergo at least N e-foldings, will scale as $T \approx Ne^{2N/3}$. We conclude that the computation time increases very rapidly with the number of e-foldings we wish to observe. The value $N = 4$ represented a practical limit to our computing resources.

APPENDIX C: INITIALIZATIONS.

The initial beam distribution function was designed for a constant linear growth rate over almost all of the unstable, positive-slope velocity range, by piecing together the simple functions([19]):

$$f_0(v) = \begin{cases} A(v-v_1)^2 + B(v-v_1)^3, & v_1 \le v \le v_a, \\ C_1 + C_2(1 - v_a/v), & v_a \le v \le v_b, \\ D(v-v_2)^2 + E(v-v_2)^3, & v_b \le v \le v_2 \end{cases} \tag{59}$$

In Eq.(59), the expressions in the velocity ranges (v_1, v_a) and (v_b, v_2) are transition functions, with the coefficients chosen so that $f_0(v)$ and $f_0'(v)$ are continuous everywhere. The coefficients are further chosen to satisfy the normalization $\int f_0(v)dv = 1$. The form (59) insures that in the interval $v_a \le v \le v_b$, the growth rate, given by Eq.(21), is constant.

A concern in choosing the coefficients e_k in Eq.(46) is to insure that the resonance overlap between adjacent modes is satisfied within the entire excited spectrum, and this from the very beginning of the simulation. Considerations of trapping widths are important because in the absence of resonance overlap there is no diffusion. In other words, the effect of the discreteness of the spectrum is attenuated only provided the modes overlap. In fact resonance overlap was satisfied in all of our simulations.

References

[1]W.E. Drummond, D. Pines, Nucl. Fusion Suppl., Part **3** (1962) 1049.

[2]J.C. Adam, G. Laval and D. Pesme, Phys. Rev. Lett., **43**, 22 (1979) 1671.

[3]G. Laval and D. Pesme, Physics Lett., **80A**, 4 (1980) 266.

[4]G. Laval and D.Pesme, Phys. of Fluids, **26**, 1 (1983) 52.

[5]G. Laval and D. Pesme, Phys. of Fluids, **26**, 1 (1983) 66.

[6]G. Laval and D. Pesme, *Phys. Rev. Letters*, **53**, 3 (1984) 270.

[7]D.F. Dubois, M. Espedal, Plasma Phys., **20** (1978) 1209.

[8]J.A. Krommes, R.G. Kleva, Phys. Fluids, **22**, 11(1979) 2168.

[9]T.H. Dupree, Phys. Fluids, **9**, 9 (1966) 1773.

[10]N.W. Murray, M.A. Lieberman and A.J. Lichtenberg, Phys. Rev. **A32**, 4 (1985) 2413.

[11]T.H.Dupree, Phys. Fluids, **15**, 2 (1972), 334.

[12]B.B. Kadomtsev, O.P. Pogutse, Phys. Fluids, **14**, 11 (1971) 2470.

[13]A. S. Bakai and Yu. S. Sigov, Sov. Phys. Dokl., **22**, 12 (1977) 753.

[14]J.M. Dawson, R. Shanny, Phys. Fluids, **11**, 1506 (1968).

[15]R.L. Morse, C.W. Nielson, Phys. Fluids, **12**, 2418 (1969).

[16]R.C. Davidson, in *Methods in Nonlinear Plasma Theory*, Academic Press, New York, 1972.

[17]D. Biskamp, H. Welter, Nuclear Fusion, **12** (1972) 89.

[18]J. C. Adam, G. Laval, D. Pesme, in *Proc. of the 4th International Conference on Waves and Instabilities* , (1980) Nagoya, Japan, edited by the Fusion Research Association of Japan.

[19]A. S. Bakai and Yu. S. Sigov, Sov. Phys. Dokl., **22**, 12 (1977) 734.

[20]*Idem*, Ref.(5).

[21]N. A. Krall and A. W. Trivelpiece, *Principles of Plasma Physics*, McGraw Hill, 1973, p.517.

[22]J.P. Boris, D.L. Book, in *Methods in Computational Physics*, vol. 16, p. 85, Academic Press, New York, 1976.

[23]C.Z. Cheng, G. Knorr, J. Comp. Physics, **22** (1976) 330.

[24]T.M. O'Neil, Phys. of Fluids, **17**, 12 (1974) 2249.

[25]R.B. Blackman, J.W. Tukey, *The Measurement of Power Spectra*, Dover, 1985.

TABLE 1: Simulation Parameters.

Simulation	1	2
$N_x \times N_v$	2048 × 200	1024 × 250
$\Delta x\ \Delta v\ \Delta t$	0.5 0.0232 0.2	0.5 0.00723 0.25
Initial Modes	79	77
$R_B = n_B/n_0$	$2.0\ 10^{-3}$	$7.4\ 10^{-4}$
Δv_B	1.4	1.1
$\omega_p T_{max}$	500	2875
τ_c	7.5	6.5
$\nu_{tt}^{-1}(t=0)$ (T_{max})	$100(v_k = 1.75)$ 45 "	$140(v_k = 1.0)$ 17 "
$\gamma_L^{-1}(t=0)$ (T_{max})	$450(v_k = 1.75)$ 400 "	$830(v_k = 1.0)$ 2500 "
$\tau_{<f>}(T_{max})$	$2000(v_k = 1.75)$	$1300(v_k = 1.0)$
$\nu_{tt}/\gamma_L(t=0)$ (T_{max})	$4.5(v_k = 1.75)$ 9 "	$5.8(v_k = 1.0)$ 150 "
N	1	3.25
$4\Delta v_{tt}/\Delta v_B(t=0)$ (T_{max})	$0.044(v_k = 1.75)$ 0.097 "	$0.027(v_k = 1.0)$ 0.24 "
$\delta_{diss}(T_{max})$	$4.0\ 10^{-3}$	$3.0\ 10^{-3}$

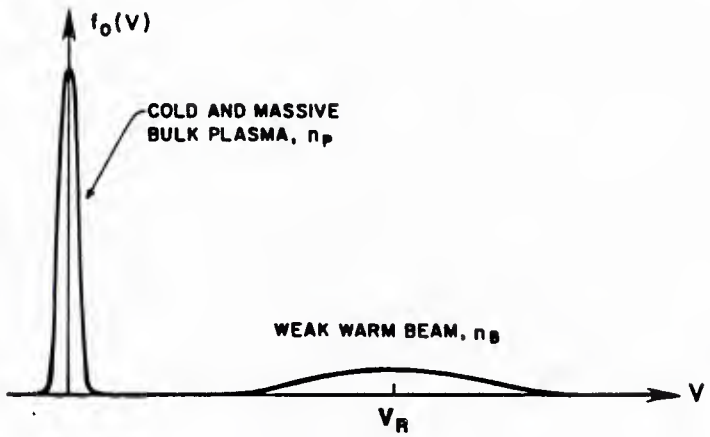

FIG. 1. Sketch of the bulk and beam distribution functions.

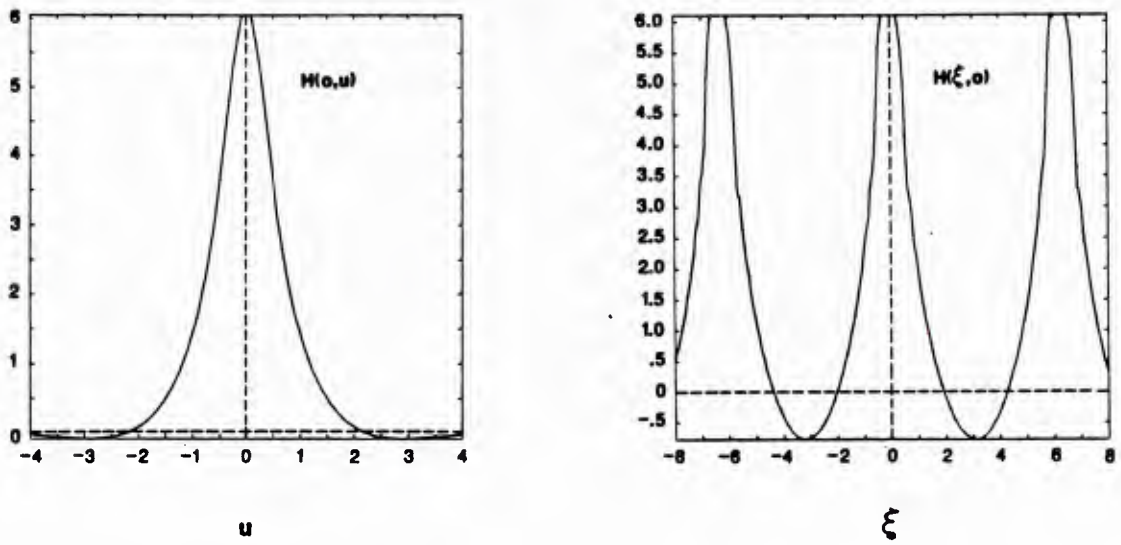

FIG. 2. (a) Plot of $H(0,u)$ showing the velocity dependence of the analytic correlation function; $u = v_-/2^{1/3}\Delta v_{tt}$. (b) Plot of $H(\xi,0)$ showing the spatial dependence of the analytic correlation function; $\xi = k_+ x_-$.

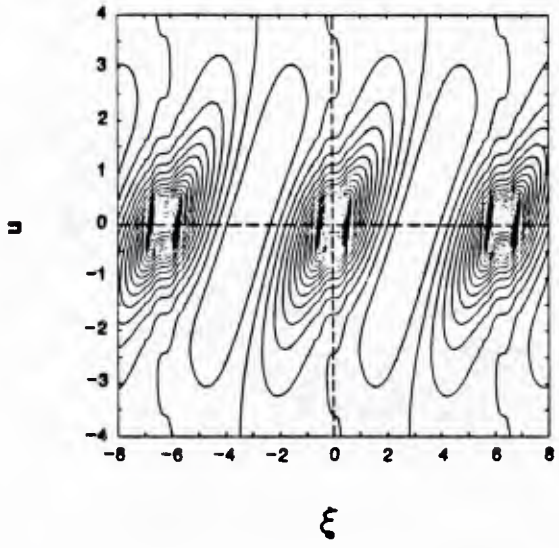

FIG. 2.(c) Contour plots of the analytic correlation function $H(\xi, u)$.

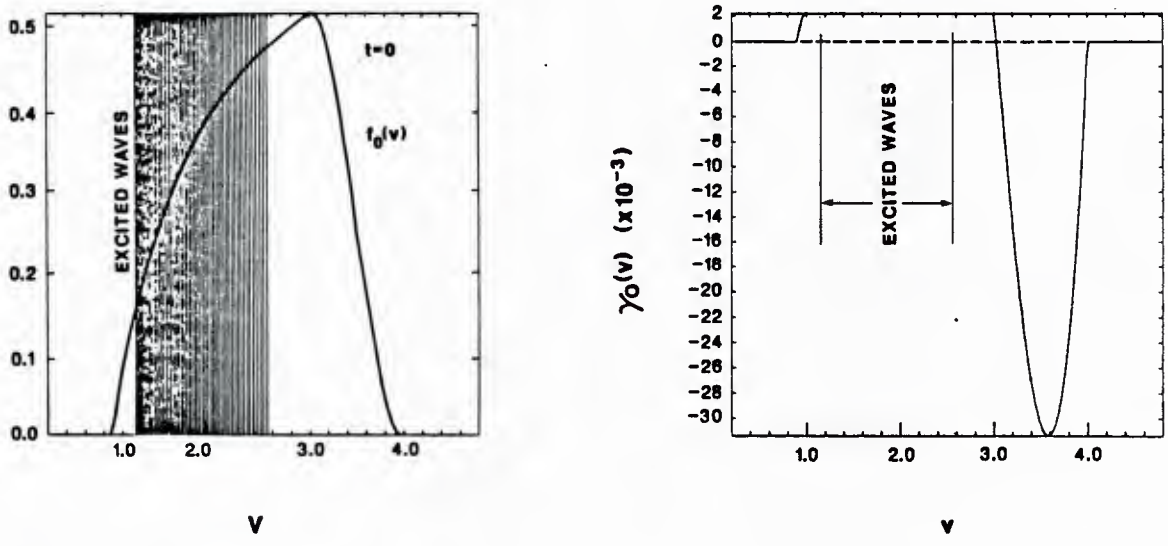

FIG. 3. (a) Initial beam distribution function $f_0(v)$ for Simulation 1 and phase velocities of the Fourier components excited at $t = 0$. (b) Initial linear growth rate for Simulation 1.

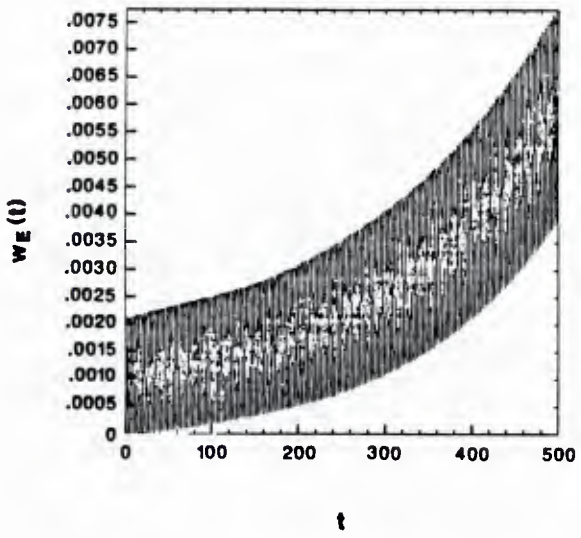

FIG. 4. Evolution of the total electric field energy in Simulation 1.

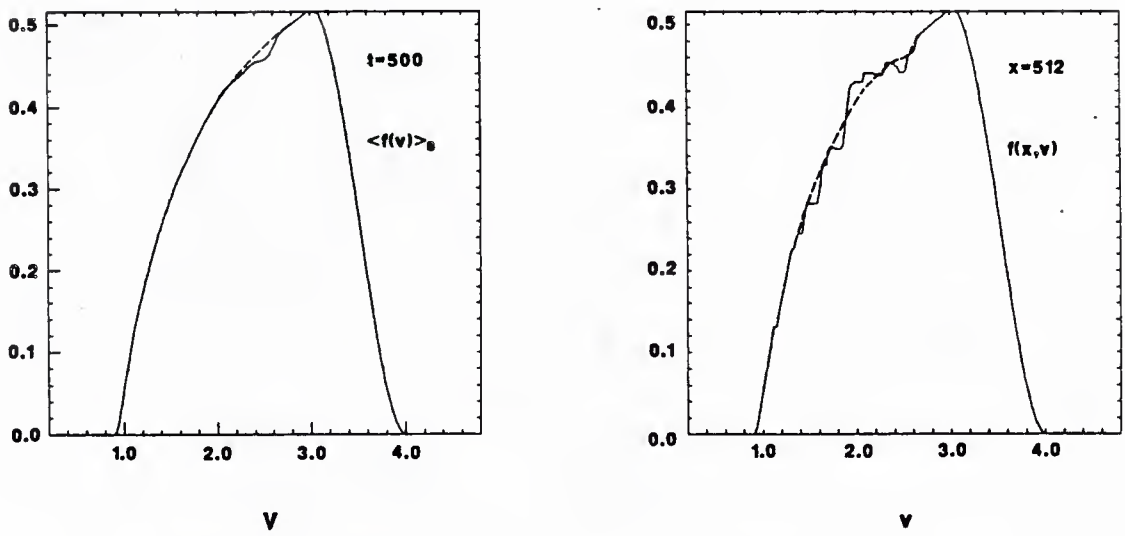

FIG. 5. Final space-averaged distribution function for Simulation 1; the dashed line is the initial space-averaged distribution function, $f_0(v)$.

FIG. 6. A cross-section of the final distribution function in simulation 1, taken at $x = 512$, showing fluctuations in f; the dashed line is the final space-averaged distribution function.

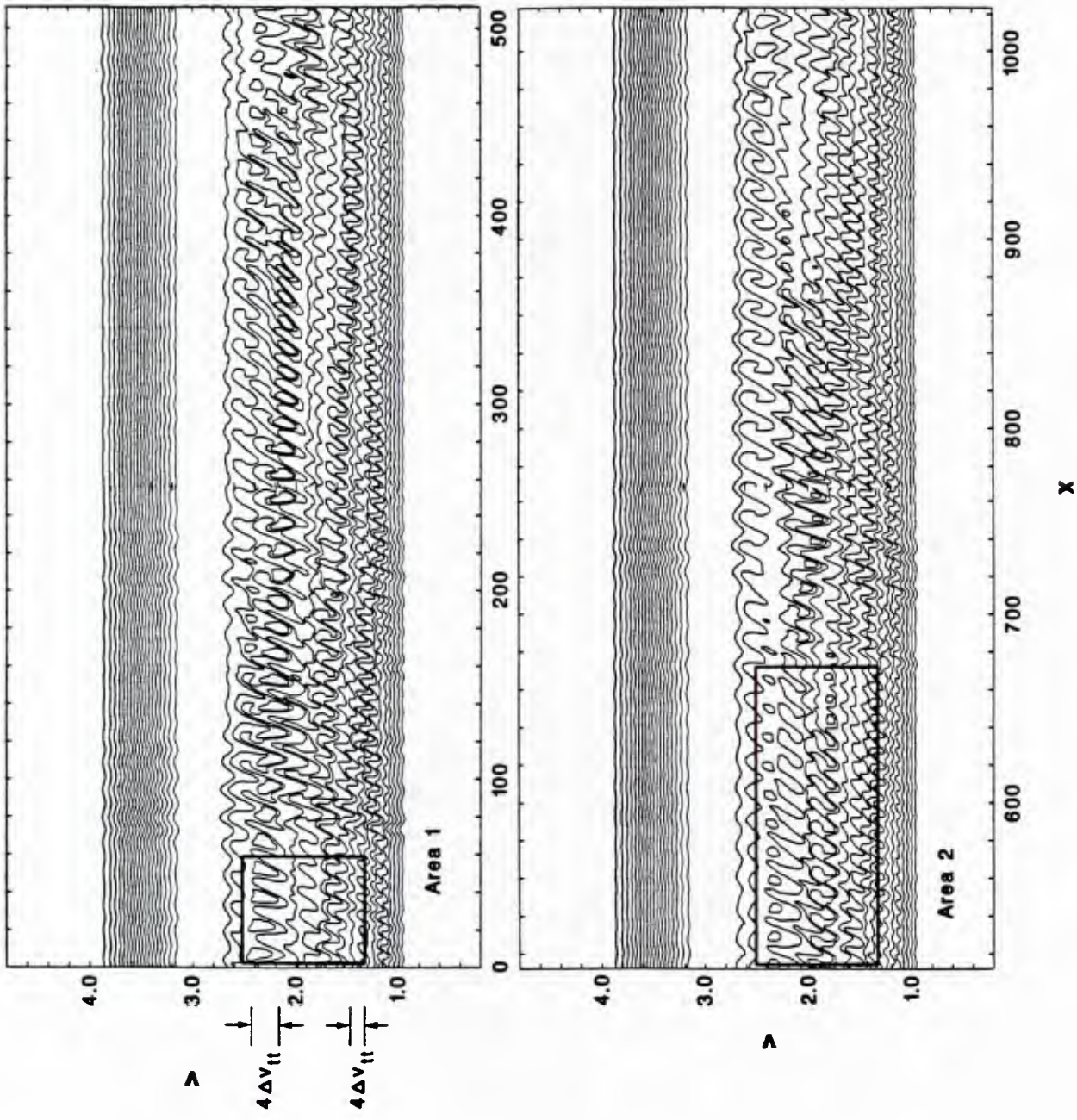

FIG. 7. Contour plot of the final beam distribution function, at $t = 500$, for Simulation 1. The total system length is 1024.

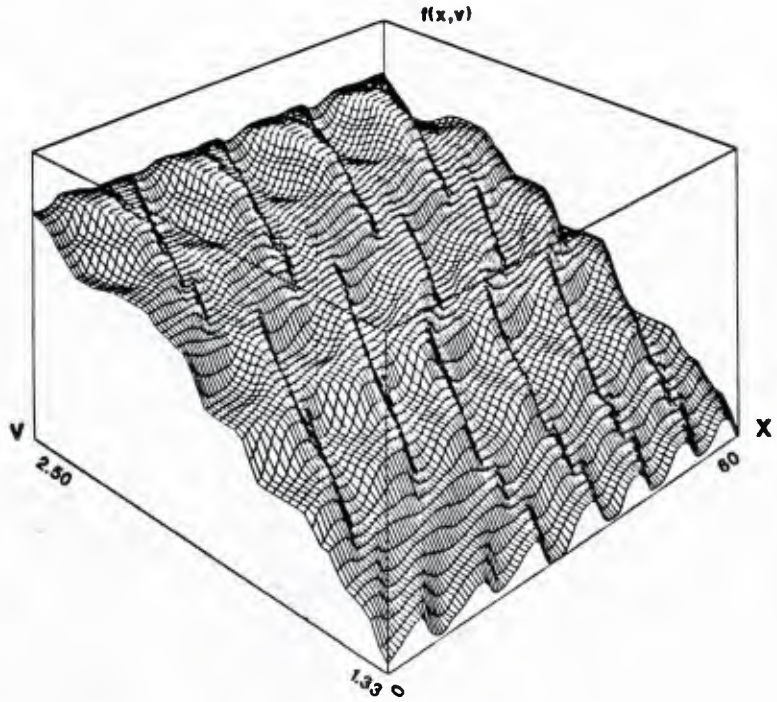

FIG. 8. Perspective view of the beam distribution function in Area 1 of Fig.(7). Note the plateaus which have formed in the distribution function.

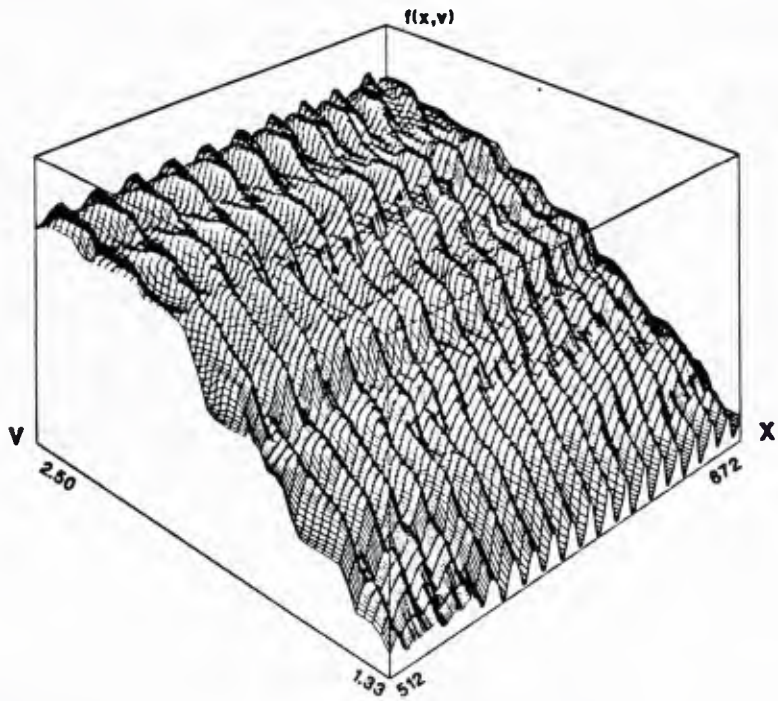

FIG. 9. Perspective view of the beam distribution function in Area 2 of Fig.(7).

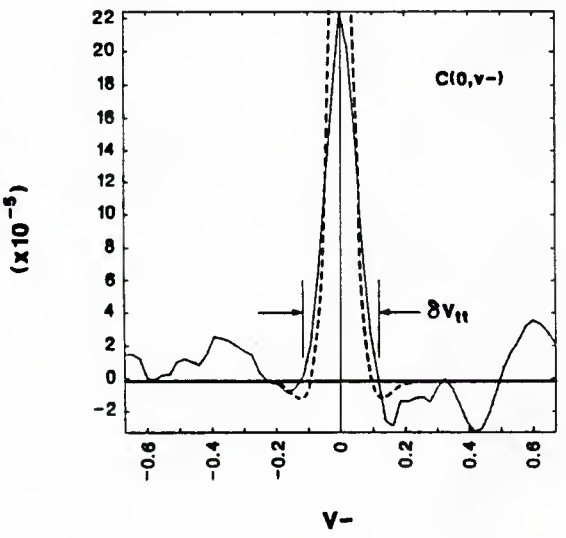

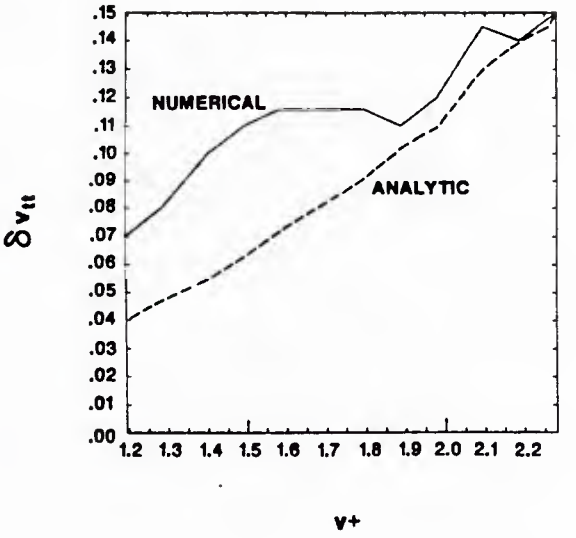

FIG. 10. Comparison of the numerical and analytic $C(0, v_-)$ for Simulation 1, for the mean velocity $v_+ = 1.745$, at $t = 500$.

FIG. 11. Comparison of the width in v_- of the function $C(0, v_-)$ (the separation of zeros at the base), plotted as a function of the mean velocity, for Simulation 1, $t = 500$. The analytic results are obtained with $\delta v_{tt} = 4.32 \Delta v_{tt}$.

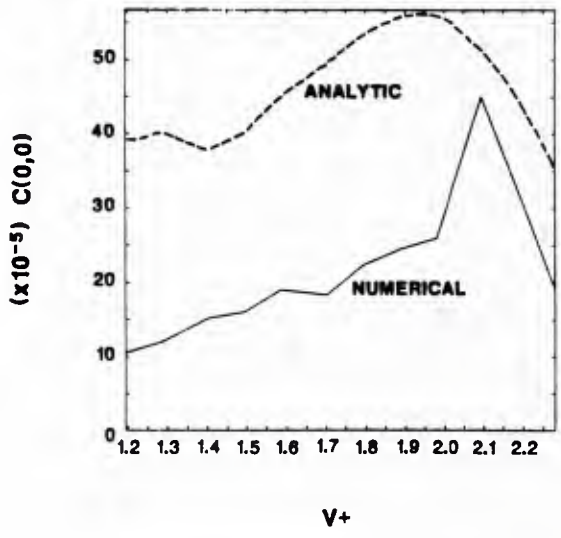

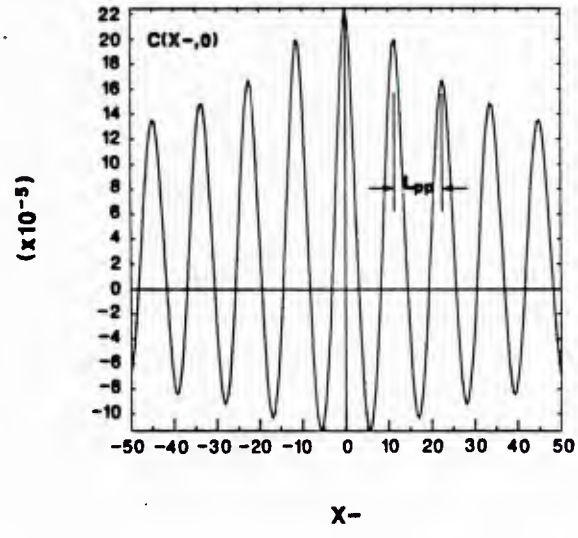

FIG. 12. Peak values $C(0,0)$ obtained in Simulation 1, $t = 500$.

FIG. 13. Plot of $C(x_-, 0)$ for $v_+ = 1.745$, Simulation 1, $t = 500$.

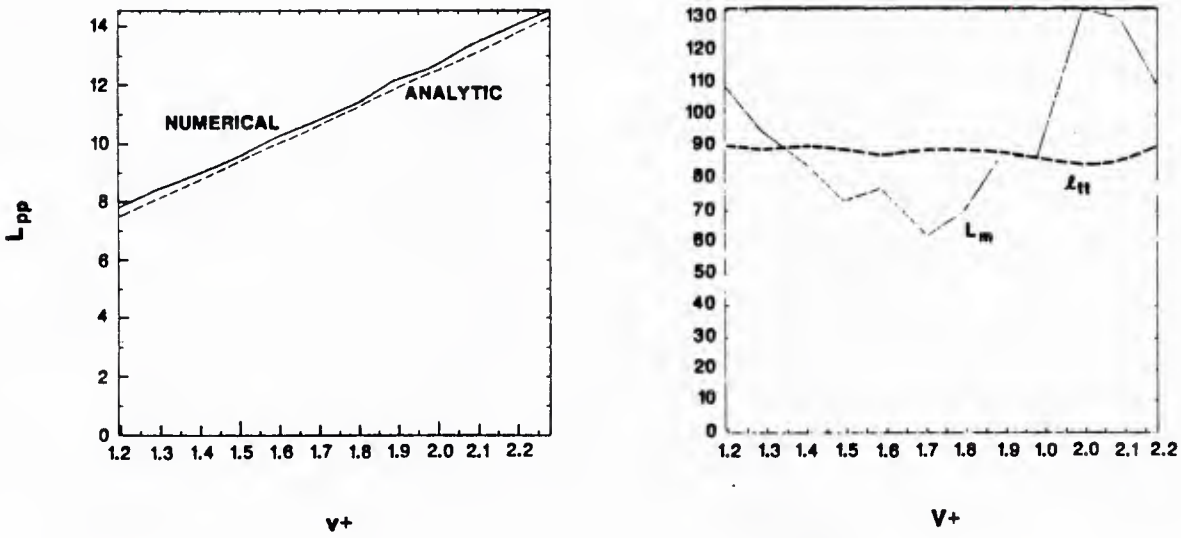

FIG. 14. Comparison of the periodicity length $\tilde{L_{pp}}$ in $C(x_-,0)$ from Fig.(13). The analytic results are obtained with $L_{pp} = 2\pi/k_+$.

FIG. 15. Comparison of numerical and theoretical spatial decay lengths for $C(x_-,0)$ from Fig.(13), The analytic result is obtained with $l_{tt} = 1/k_+^{5/3}D^{1/3}$.

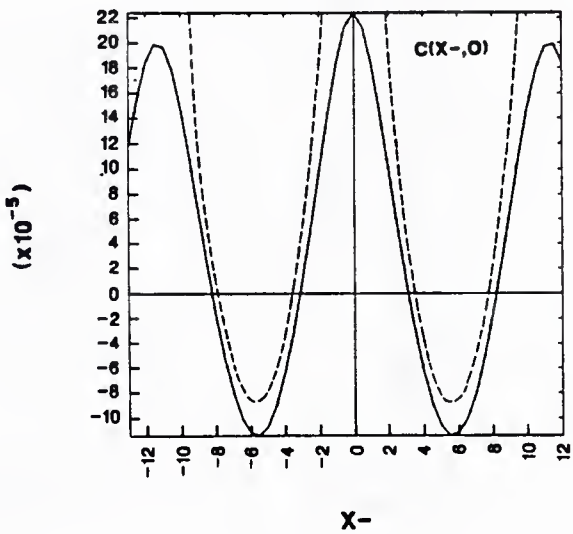

FIG. 16. Plot of $C(x_-,0)$ for $v_+ = 1.745$, Simulation 1. This is a blow-up of Fig.(13).

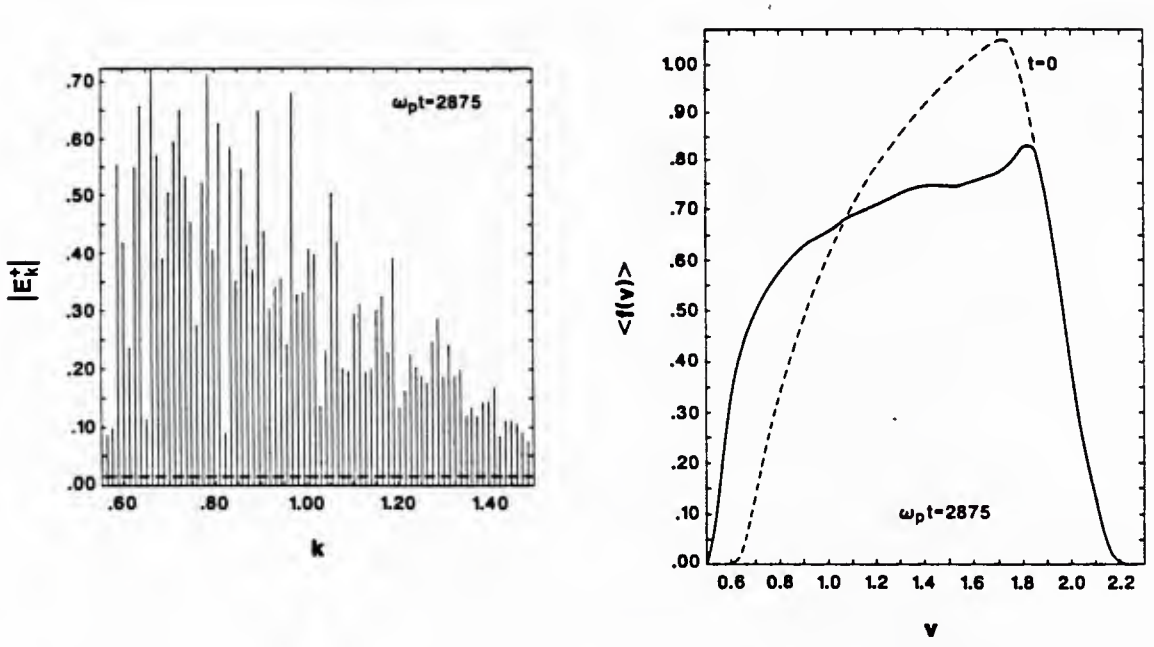

FIG. 17. The amplitude spectrum $\left|E_k^+\right|$ in Simulation 2, a) at $t = 0$ and b) at $t = 2875$. The dashed line denotes the Fourier amplitudes at $t = 0$.

FIG. 18. The initial and final average distribution function, as obtained in Simulation 2.

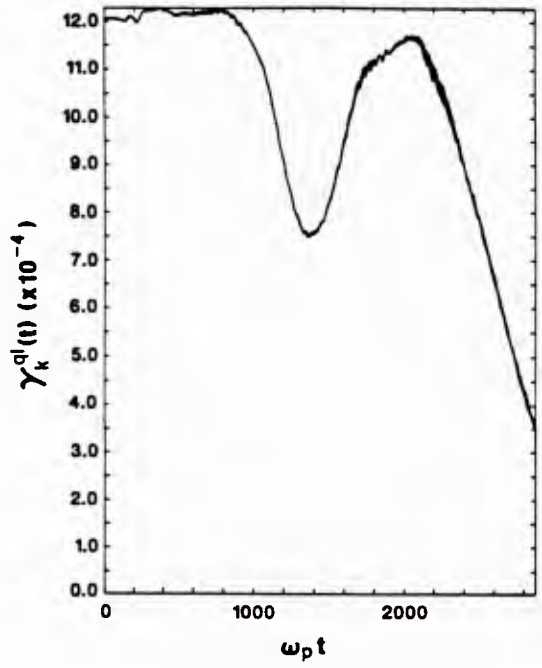

FIG. 19. Evolution of the quasilinear growth rate of the Fourier component $k = 1.0$, $v_k = 1.0$, in Simulation 2, as calculated from eq.(50).

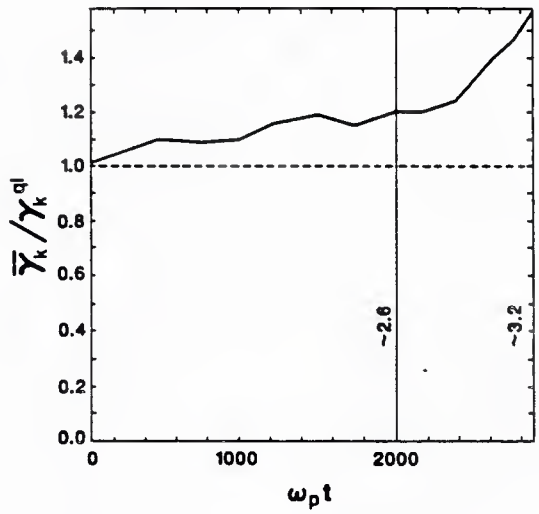

FIG. 20. Evolution of the ratio $\overline{\gamma}_k/\gamma_k^{ql}$ in Simulation 2, for $k = 1.0$. The two vertical numbers indicate the approximate number of e-foldings undergone by the field at a given time.

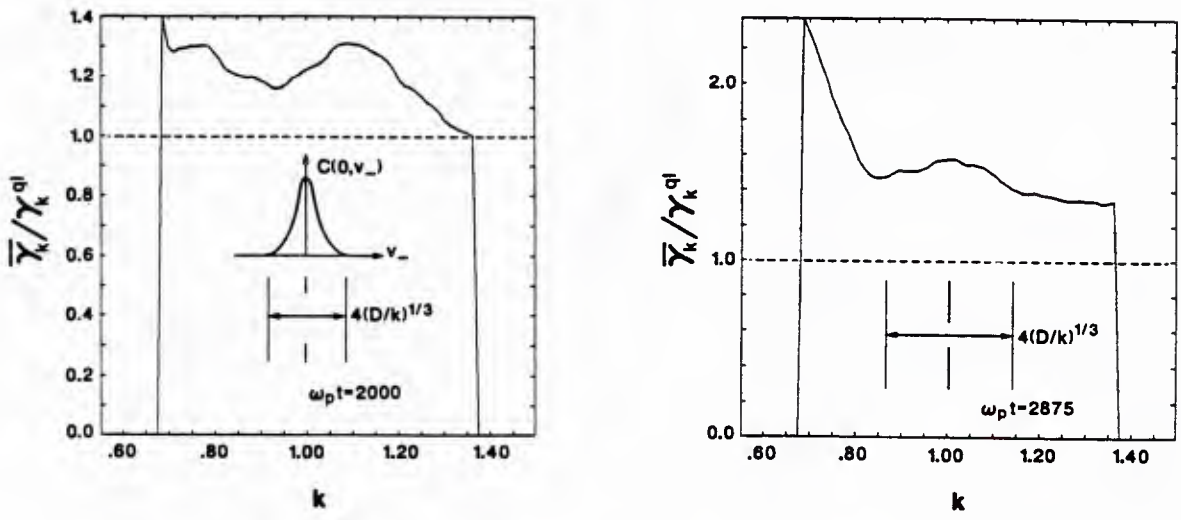

FIG. 21. The ratio of the growth rates in Simulation 2, $\overline{\gamma}_k/\gamma_k^{ql}$, plotted as a function of k for $t = 2000$. The interval indicates the range in k covered by the trapping width of waves near $k = 1.0$(the edges of the spectrum have been excluded by the averaging process which defines $\overline{\gamma}_k$).

FIG. 22. Same as Fig.(5), but for $t = 2875$.